A new approach to develop palladium-modified Ti-based alloys for biomedical applications

Qiu, Chunlei; Fones, Andrew; Hamilton, Hugh G.c.; Adkins, Nicholas J.e.; Attallah, Moataz M.

DOI:
10.1016/j.matdes.2016.07.055

Document Version
Peer reviewed version

Citation for published version (Harvard):
Qiu, C, Fones, A, Hamilton, HGC, Adkins, NJE & Attallah, MM 2016, 'A new approach to develop palladium-modified Ti-based alloys for biomedical applications', *Materials and Design*, vol. 109, pp. 98-111. https://doi.org/10.1016/j.matdes.2016.07.055

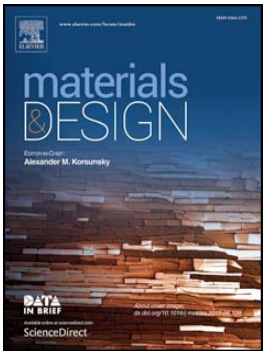

A new approach to develop palladium-modified Ti-based alloys for biomedical applications

Chunlei Qiu, Andrew Fones, Hugh G.C. Hamilton, Nicholas J.E. Adkins, Moataz M. Attallah

PII: S0264-1275(16)30955-8
DOI: doi: 10.1016/j.matdes.2016.07.055
Reference: JMADE 2059

To appear in:

Received date: 30 April 2016
Revised date: 20 June 2016
Accepted date: 12 July 2016

Please cite this article as: Chunlei Qiu, Andrew Fones, Hugh G.C. Hamilton, Nicholas J.E. Adkins, Moataz M. Attallah, A new approach to develop palladium-modified Ti-based alloys for biomedical applications, (2016), doi: 10.1016/j.matdes.2016.07.055

A new approach to develop Palladium-modified Ti-based alloys for biomedical applications

Chunlei Qiu[1,2*], Andrew Fones[3], Hugh G.C. Hamilton[3], Nicholas J.E. Adkins[1], Moataz M. Attallah[1]

[1]School of Metallurgy and Materials, University of Birmingham, Edgbaston, Birmingham B15 2TT, UK

[2]School of Engineering, Cardiff University, The Parade, Cardiff, CF24 3AA, UK

[3]Johnson Matthey Technology Centre, Blounts Court Road, Sonning Common, Reading, RG4 9NH, UK

Abstract

A new powder mixing/coating technique combined with selective laser melting (SLM) or hot isostatic pressing has been used to modify Ti-6Al-4V (Ti64) with Pd with the aim of further improving its corrosion resistance. The modified alloy samples were characterised in terms of porosity, surface structure, microstructure and composition using optical microscopy (OM), scanning electron microscopy (SEM), energy-dispersive X-ray spectroscopy (EDX) and electron microprobe analysis (EPMA). Their corrosion properties were evaluated via electrochemical tests and the mechanical properties measured via tensile tests. Using a new physical powder mixing technique, Pd was homogeneously distributed among the base Ti alloy powder particles without damaging their sphericity. After HIPing Pd is mainly located at grain boundaries while during SLM Pd has dissolved into the matrix. The porosity in the as-SLMed samples and surface roughness both increase continuously with increased laser scanning speed. Pd did not cause significant improvement in tensile properties but did enhance corrosion resistance in 2M HCl by shifting the corrosion potential into the passive region of Ti64. The current work suggested that

the new approach is a feasible route of synthesising modified alloys with both chemical and microstructural homogeneity as well as improved performance for biomedical application.

Key words: selective laser melting; hot isostatic pressing; Ti-6Al-4V; microstructure; corrosion behaviour; tensile behaviour

*Corresponding authors: Tel: (+44) 29 2087 6120; E-mail address: QiuC@cardiff.ac.uk (C.L. Qiu).

1. Introduction

Selective laser melting (SLM) is one of the additive manufacturing technologies that enable fabrication of complex freeform geometries directly from computer-aided design (CAD) models. The technology is particularly attractive for manufacturing biomedical components and structures as it allows for new complex designs that could enhance both mechanical and biomedical compatibility. So far, it has been used to fabricate a number of complex biomedical parts and structures including various porous implants [1-11], femoral components [12], human vertebra components [4] and dental parts [13]. A number of studies suggest that the selectively laser melted implants show excellent biocompatibility [1-7].

At the same time, SLM is believed to be a promising method for synthesis of new composites or modified alloys. Recently, this method has been used to prepare a number of composites for different applications [14-18]. Vrancken et al [14] used this method to process mixed powder of Ti64 and Mo and suggested that the as-fabricated samples show tensile properties that are equal to or better than conventional β-titanium alloys. Attar et al [15] synthesised in- situ Ti–TiB composites by SLM of milled Ti-TiB_2 which were found to show refined grain structure and significantly improved tensile strengths although the ductility was degraded to some extent. Gu et al [16-18] developed TiC/AlSi10Mg nanocomposites with improved microhardness and tensile strengths and TiC/Ti nanocomposites with enhanced wear resistance by SLM. The report on using this new technique to enhance performance of existing biomaterials such as their corrosion resistance and biocompatibility, however, is lacking.

The key step to produce chemically and microstructurally homogeneous composites through SLM is powder mixing. So far, most of the powder mixing has been performed by ball milling

which could easily damage the sphericity of original base alloy powder particles and also does not guarantee homogeneous distribution of the additive particles [14-16]. Very often, agglomeration of additive particles (especially nanoparticles) could still be observed and the added fine particles are usually separated from the main alloy powder particles after mixing [14-16]. These factors will all affect the distribution of additive particles among main alloy powder particles during the powder spreading stage of the SLM process and thus affect the consistency of microstructure and properties. An effective powder mixing method should not only give rise to homogeneous distribution of mixed powder particles but also keep the main alloy powder particles intact after mixing, particularly retaining the regular/spherical particle morphology that is preferable for SLM. Ideally, the additive particles should develop good bonding with main alloy powder particles after mixing so that they could be homogeneously spread with main alloy powder particles during SLM. This is particularly important for synthesis of a composite or modified alloy where the additive material is at low level. If the mixing method is not sufficiently effective, the additive material will not be widespread throughout the main alloy powder particles and the resultant SLM-built component. There are a number of such cases where the additive material is at low level in the field of biomaterials, for example, Pd-modified titanium and its alloys where Pd is usually added at a level of 0.04–0.25 wt.% [19-20]. Low level addition of Pd or other platinum group metals to titanium and its alloys is an effective way to improve corrosion resistance in a range of media, particularly reducing acids [21–24]. The conventional manufacturing route (casting + forging + machining) involves considerable waste of materials and expensive machining, which makes the production of Pd-modified titanium alloy parts for a limited number of applications expensive and time consuming. In the current study, a new powder mixing technique which involves no use of balls but only the use of

mechanical centrifugal forces and has been proven to be effective in mixing different powder particles to a very homogeneous level within a short time (several minutes) and is capable of developing good bonding among different types of powder particles [25], has been used to mix Ti64 and Pd powder particles. The mixed powder is then processed by both SLM and HIPing, the latter being used both to remove porosity from SLM-made components and because it is another effective net-shape manufacturing technology when combined with modelling [26-27]. Samples were characterised in terms of porosity, surface structure, microstructure, mechanical and chemical properties. Throughout this study, the feasibility of the proposed new route in synthesising modified biomaterials will be discussed.

2. Experimental

The base alloy powder used in this study is Grade 5 gas-atomised Ti64 powder supplied by TLS Technik in the size range of 45-75μm. The as-received Ti64 powder was doped with 0.2wt.% Pd by Johnson Matthey (JM) using a proprietary powder mixing machine that involves the use of dual centrifugal forces as shown in Figure 1. The machine mainly consists of a bottom plate and a basket set up on the plate in a slanted angle. Powder is loaded in a container which is then placed in the basket prior to mixing. When it runs, the bottom plate rotates clockwise around its central axis at an extremely high speed (up to 3500r/min) while the basket rotates anti-clockwise at a quarter of the rotation speed of the plate. As such, two dual asymmetrical forces are created which drives the powder mixing. In the current study, the powder was mixed at a rotation speed between 2500r/min and 3500r/min for only several minutes. The as-received Ti64 and mixed Ti64 and Pd powder were subsequently processed using a Concept Laser M2 Cusing SLM system which employs an Nd:YAG laser with a wavelength of 1075 nm, a maximum laser output

power of 400 W and a maximum laser scanning speed of 4300mm/s. In the current study, 10x10x10mm cubic samples have been fabricated at a constant laser power of 400W but with different laser scanning speeds ranging from 1300mm/s to 4300mm/s. All the samples were fabricated using an "island scanning" strategy which has been detailed elsewhere [28]. Selected powder samples and SLMed samples were also hot isostatically pressed at 930℃/ 100MPa/2hours followed by furnace cooling for comparison.

Samples were ground using grinding papers successively from 240 grit up to 2500 grit before being polished using 3μm diamond suspension and finally activated colloidal silica solution and examined using an optical microscope (OM) and a JEOL 7000 FEG-SEM (scanning electron microscope) to reveal the size, distribution and morphology of pores. Tessellated micrographs each containing tens of frames were used to study the porosity distribution over large areas. The porosity area fraction (A_f) was quantified using ImageJ. Samples were further etched in Kroll's reagent containing 50 ml distilled water, 25 ml HNO_3 and 5 ml HF for microstructural characterisation using OM and backscattered electron SEM. The uppermost external surfaces of the as-fabricated samples, i.e., those formed during the final powder-spread/laser-melting cycle, were also investigated using SEM. The roughness of the uppermost surfaces was measured by surface profilometry in a Surfcorder SE 1700 machine. For each sample, at least three scans were made to get an average value of surface roughness.

To study the influence of the addition of Pd on the corrosion properties of Ti64, electrochemical tests have been carried out on as-polished samples fabricated using different processes in a 1.5 litre glass cell, using a saturated calomel reference electrode (SCE) and a platinum foil counter electrode (~7 cm^2 area). The samples were mounted in resin, ground flat on successively finer

SiC papers to 4000 grit before polishing with a peroxide doped alumina polish. Coverlac stopping lacquer was used to cover all the surface but a 0.5 cm^2 area. The testing solution was 2M HCl, deaerated by argon bubbling for 1 hour before the sample was placed in the cell, with deaeration continuing throughout the experiment. Measurements were taken using a GILL12 potentiostat, with potentiodynamic sweeps performed at 0.5 mV/s. To understand the corrosion mechanisms of different samples, all the corroded sample surfaces were investigated using OM and SEM with some of the sample surfaces being studied by electron microprobe analysis (EPMA) before and after corrosion testing to understand the compositional change on sample surfaces during corrosion.

Elongated blocks (70x10x10mm) were horizontally built at 400W-2300mm/s using the M2 Cusing SLM with some being subsequently subjected to post-build HIPing at the conditions given earlier. The so-obtained samples were then machined into suitable specimens for tensile testing. The tensile tests were performed at room temperature using a computer-controlled electric screw driven Zwick/Z100 tensile testing machine and the tests were conducted under strain control mode at a strain rate of $1.0x10^{-3}$ s^{-1}. Tensile fracture surfaces were examined using SEM.

3. Results

3.1 Powder characterisation

Figure 2 shows the Ti64 powder particles and Pd distribution on the surfaces after powder mixing. The Ti64 powder particles remain spherical without observable damage. The majority of the Ti64 powder particles still show a size of 40-70μm in diameter after mixing, consistent with

the as-received Ti64 particle size range (45-70μm). Pd particles (bright particles) were found to homogeneously distribute among the Ti64 powder particles and develop good bonding with the Ti64 powder particles. This is significant for the development of new alloys and composites with good chemical and microstructural homogeneity and consistent properties through either powder metallurgy or additive manufacturing processes.

3.2 Structural integrity and microstructure

Figure 3 shows the dependence of porosity in as-fabricated Ti64-0.2Pd SLM samples on laser scanning speed at 400W. The porosity increases continuously with increased laser scanning speed, which is similar to the dependence of porosity on scanning speed for Ti64 during SLM [29]. Particularly, when the laser scanning speeds are beyond 3000mm/s, the porosity level increases significantly. Since the porosity development is believed to be associated with melt flow behaviour [29-31], the uppermost surface roughness and structure of the as-fabricated samples, which contains information about the melt flow patterns, were also investigated and the results are shown in Figure 4 and Figure 5. As Figure 4 shows, the final laser-scanned tracks on the uppermost surfaces of the as-fabricated samples become increasingly irregularly-shaped at the higher laser scanning speeds. At 1300mm/s, the laser-scanned tracks are relatively evenly spaced and homogeneously overlapped with neighbouring tracks. At 2300mm/s the tracks become increasingly misaligned and irregularly-shaped, suggesting that the melt flow became increasingly unstable. At 3800mm/s, the uppermost surface starts to show open pores and discontinuities (Figure 4(c)). The irregularity of the surface structure becomes more pronounced when the laser scanning speed is 4300mm/s (Figures 4(d)-(f)) where the discontinuities on the laser-scanned tracks becomes more frequent and the number of cave-like pores rises sharply. As a result, the uppermost surface roughness increases with increased laser scanning speed (Figure

5).

To investigate the influence of Pd on the microstructure and properties, Ti64 samples with and without Pd have been studied. Figure 6 shows the microstructure of Ti64 and Ti64-0.2Pd samples produced using different processes. It is clear that the forged+heat treated Ti64 sample generally consists of equiaxed α grains with β phase mainly located at the "triple- points" of the α grains. The as-HIPed Ti64 and as-HIPed Ti64-0.2Pd samples both show fine equiaxed α grains (average grain diameter of 6-9 μm) with β lamellae present both at the α grain boundaries and within the α grains (Figure 6(b) and Figure 7(a)) whereas the laser- processed Ti64 and Ti64-0.2Pd samples both show well-developed columnar prior β grains (average grain width of 30-100 μm). The as-SLMed Ti64 and Ti64-0.2Pd samples are generally dominated by martensitic needles while the SLMed+HIPed samples show a lamellar α+β microstructure within prior β grains.

To understand the Pd distribution within HIPed and laser fabricated Ti64-0.2Pd samples, both EPMA and EDX analysis have been performed. Figure 14 and Figure 15 show the EPMA analysis results for Pd distribution within the as-HIPed and as-SLMed Ti64-0.2Pd samples, respectively. No obvious Pd could be detected in the as-HIPed sample according to the EPMA analysis. Backscattered electron SEM imaging and EDX analysis (Figure 7) indicate that Pd exists mainly along grain boundaries as discrete particles (the bright particles in Figure 7(b)) and occasionally within some grain boundary β phase in the as-HIPed sample. In contrast, the EPMA analysis indicates that Pd is homogeneously distributed throughout the as-SLMed Ti64-0.2Pd sample, suggesting that Pd may have been completely melted and dissolved into the Ti64 matrix during SLM. The backscattered electron SEM analysis (Figure 8) does not show widespread Pd contrast throughout the sample probably due to the fact that Pd addition is very low and it has

been dissolved into the matrix. However, occasionally, there are still some regions where Pd could be observed by backscatter electron SEM imaging (Figure 8(b) and Table 1).

3.3 Tensile behaviour

Figure 9 shows the tensile properties of Ti64-0.2Pd samples prepared using different processes. Among all the samples, the as-SLMed (2300mm/s) Ti64-0.2Pd sample shows the highest strengths with 0.2% yield strength (YS) of 950MPa and ultimate tensile strength (UTS) of 1020MPa but lowest elongation of 8%. HIPing improves the ductility but also causes reduction in strengths, which is consistent with previous report on Ti64 [28]. The as- HIPed samples show the highest elongation and comparable strengths relative to the SLMed +HIPed samples. The addition of Pd was found not to cause significant change in tensile properties as evidenced by the fact that the SLMed+HIPed Ti64 sample shows comparable strengths and elongations as the SLMed+HIPed Ti64-0.2Pd sample. As compared with wrought Ti64 which could show a 0.2% YS of 875MPa, a UTS of 925MPa and an elongation of around 20% [32], the current as-SLMed Ti64-0.2Pd obviously show better strengths but poorer ductility while the SLMed+HIPed Ti64-0.2Pd samples show slightly lower strengths (0.2% YS of 830MPa and UTS of 870MPa) which could be attributed to the coarsened microstructure after HIPing.

Figure 10 shows the fracture surfaces of different Ti64-0.2Pd samples after tensile testing. The as-SLMed sample (Figure 10(a-b)) shows a fracture surface containing quite a few steps which are likely to be due to a faceted and planar fracture. Apart from that the majority of the surface area seems to be fairly smooth at micron level as compared with the samples that have been HIPed (Figure 10(c-f)) where a large number of fine dimples are widespread throughout their

fracture surfaces creating rougher surfaces at micron level, suggesting more ductile fracture during tensile testing.

3.4 Corrosion behaviour

To investigate the influence of Pd addition and manufacturing process on the corrosion resistance of Ti64, electrochemical testing has been undertaken in 2M HCl at room temperature on both Pd-free and Pd-modified Ti64 samples produced by SLM and HIP processes. Polarisation curves for these samples are shown in Figure 11. It is obvious that the as-HIPed Ti64 shows a corrosion behaviour similar to the commercial wrought counterpart (Figure 11(a)), both exhibiting an active anodic corrosion region before moving to the passive region in the first two sweeps. After that, the corrosion potential (or open circuit potential (OCP)) directly moves into the passive region of Ti64 without experiencing an active anodic region, suggesting that the passive films developed in the first couple of sweeps have become highly corrosion resistant. The as-SLMed Ti64, in contrast, shows an increased OCP, resulting in no active anodic corrosion region on the early sweeps. Instead it goes directly into the passive region, implying that the as-SLMed microstructure is more corrosion resistant than wrought or HIPed samples probably due to its much coarser grain structure and more homogeneously and densely distributed β lamellae. Pd addition also helps shift the corrosion potential into the passive region for Ti64 (see Figure 11(d)-(g)), thereby eliminating the active anodic region. Moreover, it is noted that the SLM-processed Ti64-0.2Pd samples (Figures 11(e)-(g)) tend to show more consistent polarisation behaviour than the as-HIPed counterpart in different sweeps, implying that the former may have developed more stable passive films from the very beginning of the

electrochemical test. The sample fabricated at higher laser scanning speed (Figure 11(f)) which contains more porosity was found to show increased OCP but comparable passive current as those with lower porosity (Figure 11(e), suggesting the influence of pores on corrosion resistance in the current solution was not manifested during these tests but longer term and more extensive testing is needed.

The electrochemically tested samples were also studied using OM, SEM and EPMA and the results are shown in Figures 12-15. All the samples experience a certain level of attack during the testing, but the extent is quite different. The wrought and as-HIPed Ti64 samples obviously have undergone severe attacks with a number of grains having been corroded away (Figures 12(a)-(b)). Within the surface of the as-SLMed Ti64, only some large columnar grains were dissolved (see Figure 12(c)). In contrast, the Pd-containing samples (Figure 12(d)-(f)) do not show obvious dissolution of grains and instead only some of the lamellar α have been attacked and removed. As for the sample containing higher porosity (fabricated at 3300mm/s), the pores show no obvious change in size, morphology and internal surface structure after corrosion (Figure 13) indicating that the pores are not necessarily preferential corrosion attack sites. EPMA analysis on sample surfaces before and after corrosion testing reveals no obvious change in composition (Figures 14-15; left- vs. right-hand columns), suggesting that the corrosion behaviour depends greatly on the composition of the material itself. It is also noted that the as-SLMed Ti64-0.2Pd sample shows more Pd but less Al on the sample surface as compared with the as-HIPed sample, probably due to more homogeneous distribution of Pd in the former case.

4. Discussion

The current experimental results demonstrate that the laser scanning speed shows significant

influence on porosity and surface structure development for Ti64-0.2Pd samples during SLM. With the increase of laser scanning speed, the internal porosity increases continuously and the surface structure becomes increasingly irregularly-shaped and complicated with the development of surface pores and discontinuities. The latter obviously indicate increasingly unstable melt flow with increased laser scanning speed. A similar phenomenon was observed in previous work on SLM of Ti64 and Invar 36 where increases in laser scanning speeds increased the flow velocity and instability of the melt pool [29-31]. Unstable melt pools tend to raise material away from the build surfaces rather than allow it to spread steadily along laser scanning direction [29], which is liable to cause development of cave-like pores (Figure 4(e-f)) and elongated pores at the interfaces between layers as observed in Figure 3(c). Moreover, at a constant laser power but with increased laser scanning speed, the input energy density would become smaller and it is more likely that the previously deposited layer is not sufficiently remelted and bonded with the fresh layer, leading to poorer mechanical integrity.

The use of the new powder mixing technique was found to have not only homogeneously mixed two types of powder particles but also deformed the Pd particles such that they bond to the main Ti alloy powder particles without damaging the sphericity of the latter. This is very important for synthesis of composites or modified alloys through powder metallurgy or additive manufacturing as one of the major concerns has been to ensure the microstructural and chemical homogeneity and powder mixing is the key step to achieve the goal. The short powder mixing duration (at a level of several minutes) is probably the principal factor in reducing the opportunity for deformation of the base Ti64 powders. The development of bonding between two dissimilar types of powder particles is believed to be due to the difference in their mechanical properties such as hardness and malleability. As Pd particles are more malleable than Ti64 particles, they

may have been smashed by the centrifugal force and coated over the Ti64 particles as observed in Figure 2.

The added Pd exists as particles mainly located at grain boundaries in as-HIPed samples but was found to be completely dissolved into the matrix of the main alloy with homogeneous distribution after SLM. The addition of Pd did not change tensile properties significantly but did lead to great improvement in corrosion resistance by shifting the corrosion potential into the passive region for Ti64 (Figure 11), thereby eliminating the active anodic region where high corrosion rates occur. In addition, the processing technique also influenced the corrosion behaviour, particularly in the absence of Pd, by affecting microstructural development. The forging and HIPing processes, which tend to develop fine equiaxed α grains of several microns in diameter in Ti64 samples, both gave rise to active anodic regions during electrochemical testing due to the preferential corrosion along grain boundaries, as evidenced by the observation on the corroded surfaces (Figure 12(a)-(b)). SLM processing, which led to the development of large columnar grains with widths of tens and even hundreds of microns and of more homogeneously and densely distributed β lamellae which is relatively more corrosion resistant than α, however, avoided the development of active anodic regions (Figure 12(c)). With the addition of Pd, even the as-HIPed sample did not display the active anodic stage, probably due to the presence of Pd at grain boundaries which has improved the corrosion resistance there (Figure 7(b)). It is noted that there is no obvious change in composition on sample surfaces before and after corrosion in the present study (Figures 14-15). This seems to be different from previous studies which suggest that, during corrosion periods, Pd would be enriched in the sample surface either by preferential dissolution of Ti [33-36] or dissolution of both with subsequent redeposition of Pd on the corroded surface [23]. The difference may be due to the fact that in the

current work, the Ti64 and Pd powders have been homogeneously distributed, which thus gave rise to more homogeneous distribution of Pd in the as-SLMed sample (as evidenced in Figure 15) that is beneficial for development of strong passive film in the very beginning of corrosion. As for the as-HIPed sample, Pd may have still been localised at grain boundaries even after corrosion, and the damage seen is slight enough not to have dissolved out entire grains, hence no further grain boundary Pd has been revealed. The difference in the distribution of Pd in the as-SLMed and as-HIPed samples is also believed to account for the difference in corrosion behaviour. The former show more consistent corrosion behaviours during sequential sweeps when compared with the latter, as shown in Figures 11(d)-(e)), with more homogeneous distribution of Pd in the former sample probably having helped develop a stronger and more stable passive film from the very beginning of corrosion test.

The presence of a certain level of porosity in as-SLMed Ti64-0.2Pd samples was found not to cause significant influence on corrosion behaviour (Figure 11(e)-(f)) in the short term tests and there is no evidence to show that the pores would be the preferential attack sites during the corrosion test. This is important as it gives a wider processing window for producing these kinds of materials without compromising properties significantly, although longer term testing is clearly required.

Based on the preliminary results obtained in the present work, the new processing route, which includes the use of a new powder mixing/coating method combined with SLM or HIPing, is a feasible and efficient route to produce modified biomaterials with improvement of specific properties.

5. Conclusions

(i) The use of a new powder mixing technique led to homogeneous mixing and good bonding of Ti64 and Pd powder particles without damaging the sphericity of the former, which ensures the acquisition of both chemical and microstructural homogeneity during additive manufacturing.

(ii) The added Pd exists in the form of particles present mainly at grain boundaries after HIPing but has been completely dissolved into the matrix of Ti64 after SLM.

(iii) The addition of Pd did not change the tensile properties of Ti64 significantly but greatly improved its corrosion resistance particularly for the as-HIPed sample.

(iv) The porosity, surface roughness and irregularity of surface structure of the as-SLMed samples increase continuously with increased laser scanning speed, which is believed to be due to increasingly unstable melt flow.

(v) The presence of a certain level of porosity (around 1%) in as-SLMed Ti64-0.2Pd samples did not lead to obvious degradation of corrosion resistance.

(vi) The proposed new route, involving the combined use of a new powder mixing technique and SLM or HIPing, is feasible and efficient in producing modified titanium alloys with improved specific properties.

Acknowledgement

The work shown in this paper is part of an AccMet project (Accelerated Metallurgy) and was financially sponsored by the Seventh European Frame Programme (FP7), European Commission. A.F and H.H thank Mr. Gareth D. Hatton and Mr. W. Van Mierlo for help in EPMA and SEM analysis on corroded samples. Johnson Matthey wish to acknowledge Anglo American Platinum

for financial support.

References

[1] R. Wauthle, J. van der Stok, S.A. Yavari, J.Van Humbeeck, J.-P. Kruth, A.A. Zadpoor, H. Weinans, M. Mulier, J. Schrooten, Additively manufactured porous tantalum implants, Acta. Biomater. 14 (2015) 217–225.

[2] D.K. Pattanayak, A. Fukuda, T. Matsushita, M. Takemoto, S. Fujibayashi, K. Sasaki, N. Nishida, T. Nakamura, T. Kokubo, Bioactive Ti metal analogous to human cancellous bone: Fabrication by selective laser melting and chemical treatments, Acta. Biomater. 7 (2011) 1398–1406.

[3] J.M. Kanczler, S.-H. Mirmalek-Sani, N.A. Hanley, A.L. Ivanov, J.J.A. Barry, C. Upton, K.M. Shakesheff, S.M. Howdle, E.N. Antonov, V.N. Bagratashvili, V.K. Popov, R.O.C. Oreffo, Biocompatibility and osteogenic potential of human fetal femur-derived cells on surface selective laser sintered scaffolds, Acta. Biomater. 5 (2009) 2063–2071.

[4] D.A. Hollander, M.von Walter, T. Wirtz, R. Sellei, B. Schmidt-Rohlfing, O. Paar, H.-J. Erli, Structural, mechanical and in vitro characterization of individually structured Ti–6Al– 4V produced by direct laser forming, Biomaterials. 27 (2006) 955–963.

[5] S. Van Bael, Y.C. Chai, S. Truscello, M. Moesen, G. Kerckhofs, H. Van Oosterwyck, J.-P.

Kruth, J. Schrooten. The effect of pore geometry on the in vitro biological behavior of human periosteum-derived cells seeded on selective laser-melted Ti6Al4V bone scaffolds, Acta. Biomater. 8 (2012) 2824–2834.

[6] B. Duan, M. Wang, W.Y. Zhou, W. L. Cheung, Z.Y. Li, W.W. Lu, Three-dimensional nanocomposite scaffolds fabricated via selective laser sintering for bone tissue engineering, Acta. Biomater. 6 (2010) 4495–4505.

[7] A. Fukuda, M. Takemoto, T. Saito, S. Fujibayashi, M. Neo, D. K. Pattanayak, T. Matsushita, K. Sasaki, N. Nishida, T. Kokubo, T. Nakamura, Osteoinduction of porous Ti implants with a channel structure fabricated by selective laser melting, Acta. Biomater. 7 (2011) 2327–2336.

[8] F.X. Xie, X.M. He, Y.M. Lv, M.P. Wu, X.B. He, X.H. Qu, Selective laser sintered porous Ti–(4–10)Mo alloys for biomedical applications: Structural characteristics, mechanical properties and corrosion behaviour, Corr. Sci. 95 (2015) 117–124.

[9] J.J. de Damborenea, M.A. Larosa, M.A. Arenas, J.M. Hernández-López, A.L. Jardini, M.C.F. Ierardi, C.A.C. Zavaglia, R.M. Filho, A. Conde, Functionalization of Ti6Al4V scaffolds produced by direct metal laser for biomedical applications, Mater. Des. 83 (2015) 6–13.

[10] C.Z. Yan, L. Hao, A. Hussein, P. Young. Ti–6Al–4V triply periodic minimal surface structures for bone implants fabricated via selective laser melting. J. Mech. Behavior. Biomed. Mater. 51 (2015) 61–73.

[11] C.L. Qiu, S. Yue, N.J.E. Adkins, M. Ward, H. Hassanin, P.D. Lee, P.J. Withers, M.M. Attallah, Influence of processing conditions on strut structure and compressive properties of cellular lattice structures fabricated by selective laser melting. Mater. Sci. Eng. A. 628 (2015) 188-197.

[12] L.E. Murr, S.A. Quinones, S.M. Gaytan, M.I. Lopez, A. Rodela, E.Y. Martinez, D.H. Hernandez, E. Martinez, F. Medina, R.B. Wicker, Microstructure and mechanical behavior of Ti–6Al–4V produced by rapid-layer manufacturing, for biomedical applications. J. Mech. Behavior. Biomed. Mater. 2 (2009) 20-32.

[13] A. Takaichia, Suyalatu, T. Nakamoto, N. Joko, N. Nomura, Y. Tsutsumi, S. Migita, Hisashi. Doi, S. Kurosu, A. Chiba, N. Wakabayashi, Y. SaIgarashia, T. Hanawa, J. Mech. Behavior. Biomed. Mater. 21 (2013) 67-76.

[14] B. Vrancken, L. Thijs, J.-P. Kruth, J. Van Humbeeck, Microstructure and mechanical properties of a novel β titanium metallic composite by selective laser melting, Acta. Mater. 68 (2014) 150–158.

[15] H. Attar, M. Bönisch, M. Calin, L.C. Zhang, S. Scudino, J. Eckert, Selective laser melting of in situ titanium–titanium boride composites: Processing, microstructure and mechanical properties, Acta. Mater. 76 (2014) 13–22.

[16] D.D. Gu, H.Q. Wang, D.H. Dai, P.P. Yuan,W. Meiners, R. Poprawe, Rapid fabrication of Al-based bulk-form nanocomposites with novel reinforcement and enhanced performance by selective laser melting, Scripta. Mater. 96 (2015) 25–28.

[17] D.D. Gu, G.B. Meng, C. Li, W. Meiners, R. Poprawe, Selective laser melting of TiC/Ti bulk nanocomposites: Influence of nanoscale reinforcement, Scripta. Mater. 67 (2012) 185– 188.

[18] D.D. Gu, Y.-C. Hagedorn, W. Meiners, K. Wissenbach, R. Poprawe, Nanocrystalline TiC reinforced Ti matrix bulk-form nanocomposites by Selective Laser Melting (SLM): Densification, growth mechanism and wear behaviour, Compos. Sci. Tech. 71 (2011) 1612–1620.

[19] R. Thomas, Titanium in the geothermal industry, GHC Bull. 24 (2003) 22–26.

[20] R.W. Schutz, F.N. Speller, award lecture: Platinum group metal additions to titanium: a highly effective strategy for enhancing corrosion resistance, Corrosion. 59 (2003) 1043– 1057.

[21] M. Stern, H. Wissenberg, The influence of noble metal alloy additions on the electrochemical and corrosion behavior of titanium, J. Electrochem. Soc. 106 (1959) 759– 764.

[22] N.D. Tomashov, R.M. Altovsky, G.P. Chernova, Passivity and corrosion resistance of titanium and its alloys, J. Electrochem. Soc. 108 (1961) 113–119.

[23] J.B. Cotton, The role of palladium in enhancing corrosion resistance of titanium, Platinum Met. Rev. 11 (1967) 50–52.

[24] R.D. Armstrong, R.E. Firman, H.R. Thirsk, Ring-disk studies of titanium–palladium alloy corrosion, Corros. Sci. 13 (1973) 409–420.

[25] M.A. Ashworth, A.J. Davenport, R.M. Ward, H.G.C. Hamilton, Microstructure and corrosion of Pd-modified Ti alloys produced by powder metallurgy, Corr. Sci. 52 (2010) 2413–2421.

[26] Seliverstov D, Samarov V, Goloviskin V, Alexandrov S, Ekstrom P. Capsule design for hip of complex shape parts. In Proceedings of the International Conference on Hot Isostatic Pressing. Rotterdam, 1993.

[27] Yuan WX, Mei J, Samarov V, Seliverstov D, Wu X. Computer modelling and tooling design for near net shaped components using hot isostatic pressing, J. Mater. Proc. Tech. 2007; 182:39-49.

[28] C.L. Qiu, N. J. E. Adkins, M. M.Attallah, Microstructure and tensile properties of selectively laser-melted and of HIPed laser-melted Ti–6Al–4V, Mater. Sci. Eng. A. 578 (2013) 230–239.

[29] C.L. Qiu, C. Panwisawas, M. Ward, H.C. Basoalto, J.W. Brooks, M.M. Attallah, On the role of melt flow into the surface structure and porosity development during selective laser melting, Acta. Mater. 96 (2015) 72–79.

[30] C. Panwisawas, C.L. Qiu, Y. Sovani, J.W. Brooks, M.M. Attallah, H.C. Basoalto, On the role of thermal fluid dynamics into the evolution of porosity during selective laser melting, Scripta. Mater. 105 (2015) 14-17.

[31] C.L. Qiu, N.J.E. Adkins, M.M. Attallh, Selective laser melting of Invar 36: microstructure and properties, Acta. Mater. In press.

[32] Z.W. Wu, C.L. Qiu, V. Venkatesh, H. Fraser, R. Williams, G.B. Viswanathan, M. Thomas,

S. Nag, R. Banerjee, M.H. Loretto. The Influence of Precipitation of Alpha2 on Properties and Microstructure in TIMETAL 6-4. Metall. Mater. Trans. A. 44(2013)1706-1713.

[33] R.D. Armstrong, R.E. Firman, H.R. Thirsk, Ring-disk studies of titanium–palladium alloy corrosion, Corros. Sci. 13 (1973) 409–420. [34] G.K. Hubler, E. McCafferty, Corrosion behavior and Rutherford backscattering analysis of palladium-implanted titanium, Corros. Sci. 20 (1980) 103–116.

[35] E. Van der Lingen, The effect of micro-alloying with ruthenium or palladium on the corrosion properties of titanium in aqueous chloride environments, Ph.D. thesis, Faculty of Engineering, University of Pretoria, Pretoria, 1998. [36] E. McCafferty, G.K. Hubler, Electrochemical behavior of palladium-implanted titanium, J. Electrochem. Soc. 125 (1978) 1892–1893.

Table 1 EDX quantitative analysis resluts for as-SLMed Ti64-0.2Pd sample (at.%)

Element	Pd-rich zone-1	Pd-rich zone-2	Pd-rich zone-3	Matrix area-1	Matrix area-2
Al	8.68	8.99	8.52	8.39	8.82
Ti	87.70	87.00	87.62	87.30	88.14
V	2.64	2.80	3.26	4.31	3.04
Pd	0.98	1.20	0.60	-	-

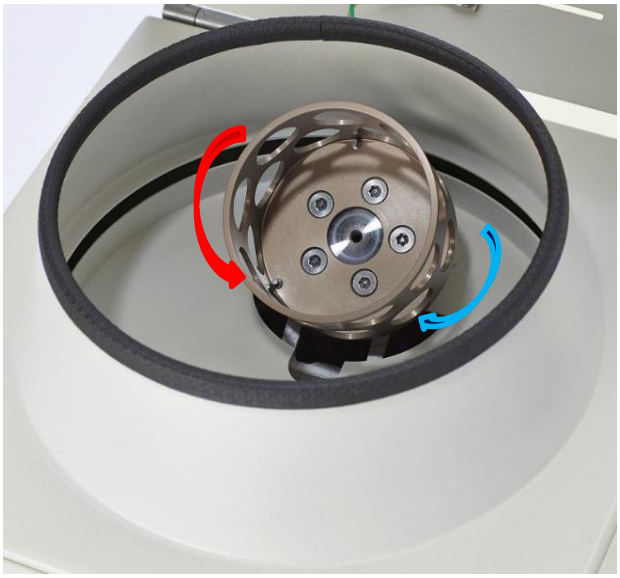

Figure 1 A photo showing the new powder mixing machine used in the current study. The arrows show the rotation of bottom plate and the basket along their axes in different directions.

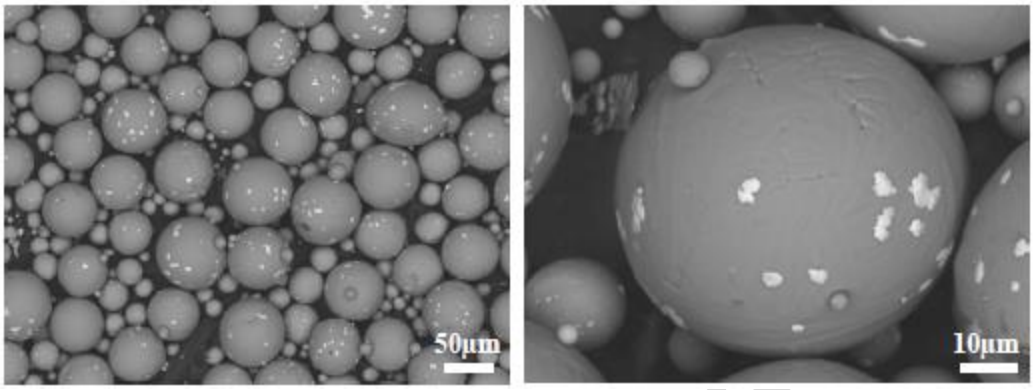

Figure 2 Back-scattered electron SEM images showing the Ti64 powder particle and Pd distribution after mixing.

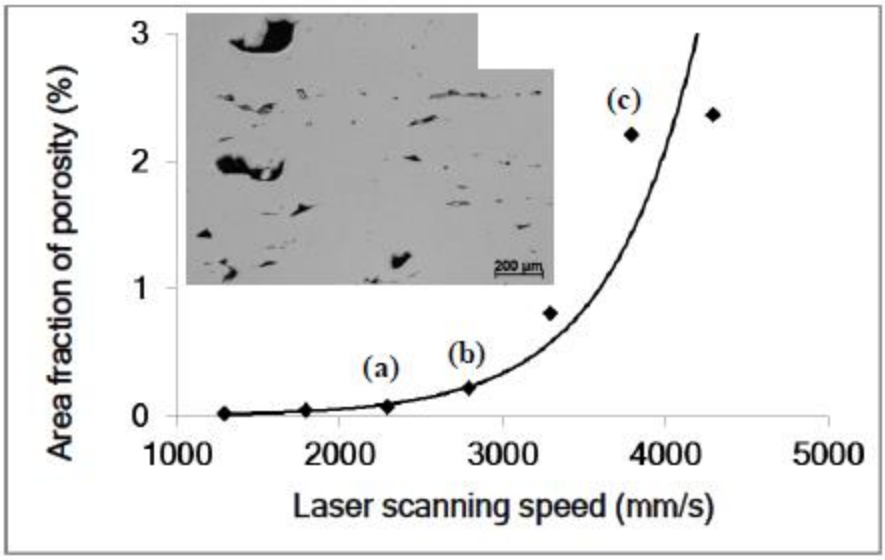

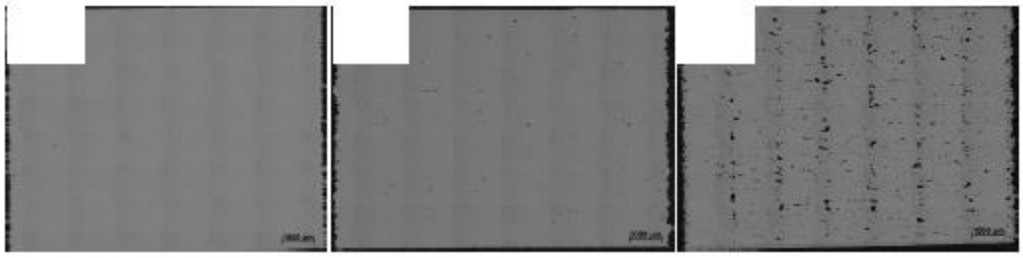

Figure 3 Plot showing the dependence of porosity on laser scanning speed and OM micrographs showing the porosity distribution within the samples fabricated at (a) 2300mm/s; (b) 2800mm/s; (c) 3800mm/s.

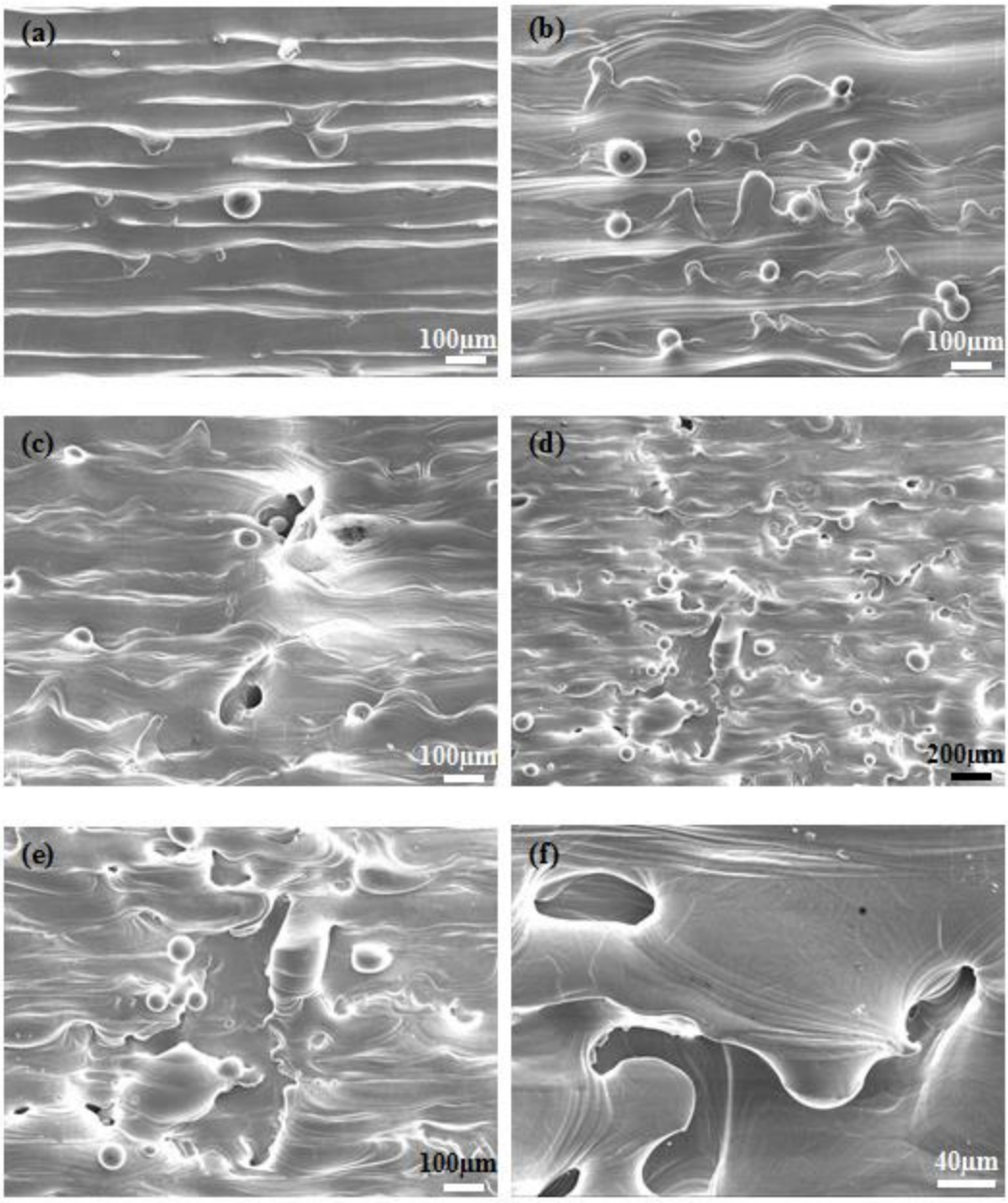

Figure 4 SEM micrographs showing the uppermost surface structure of samples fabricated at (a) 1300mm/s; (b) 2300mm/s; (c) 3800mm/s; (d)-(f) 4300mm/s.

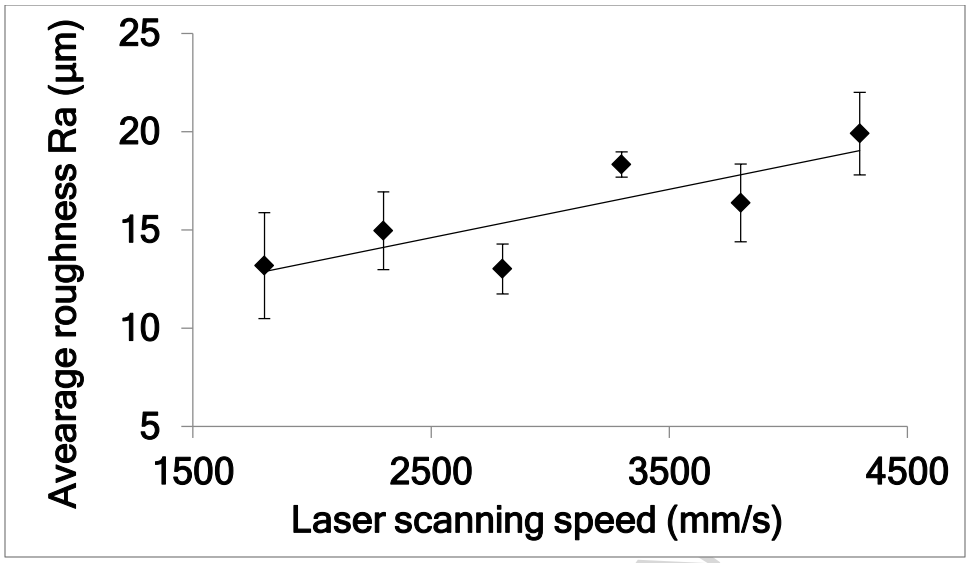

Figure 5 Plot showing the dependence of the uppermost surface roughness on laser scanning speed

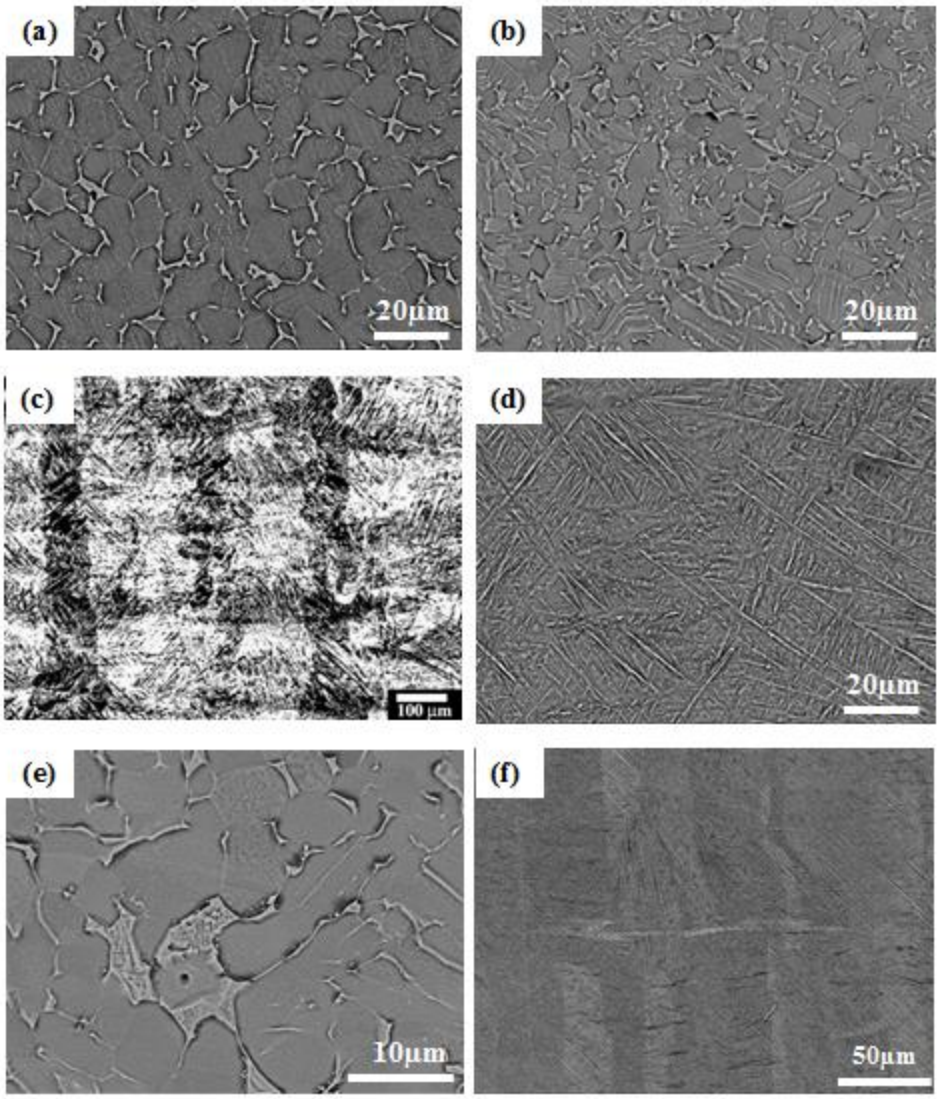

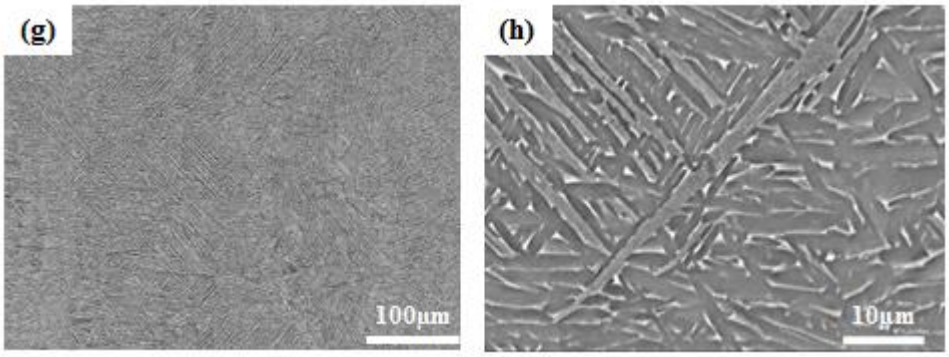

Figure 6 Back-scattered electron SEM images showing the microstructure of (a) forged + annealed Ti64 (average grain diameter *D*=9.0 μm); (b) as-HIPed Ti64 (*D*=7.0 μm); (c-d) as-SLMed Ti64 (average grain width of 85μm); (e) as-HIPed Ti64-0.2Pd (*D*= 6 μm); (f) as-SLMed Ti64-0.2Pd (average grain width of 30μm) and (g-h) SLMed+HIPed Ti64-0.2Pd samples (average grain width of 100μm).

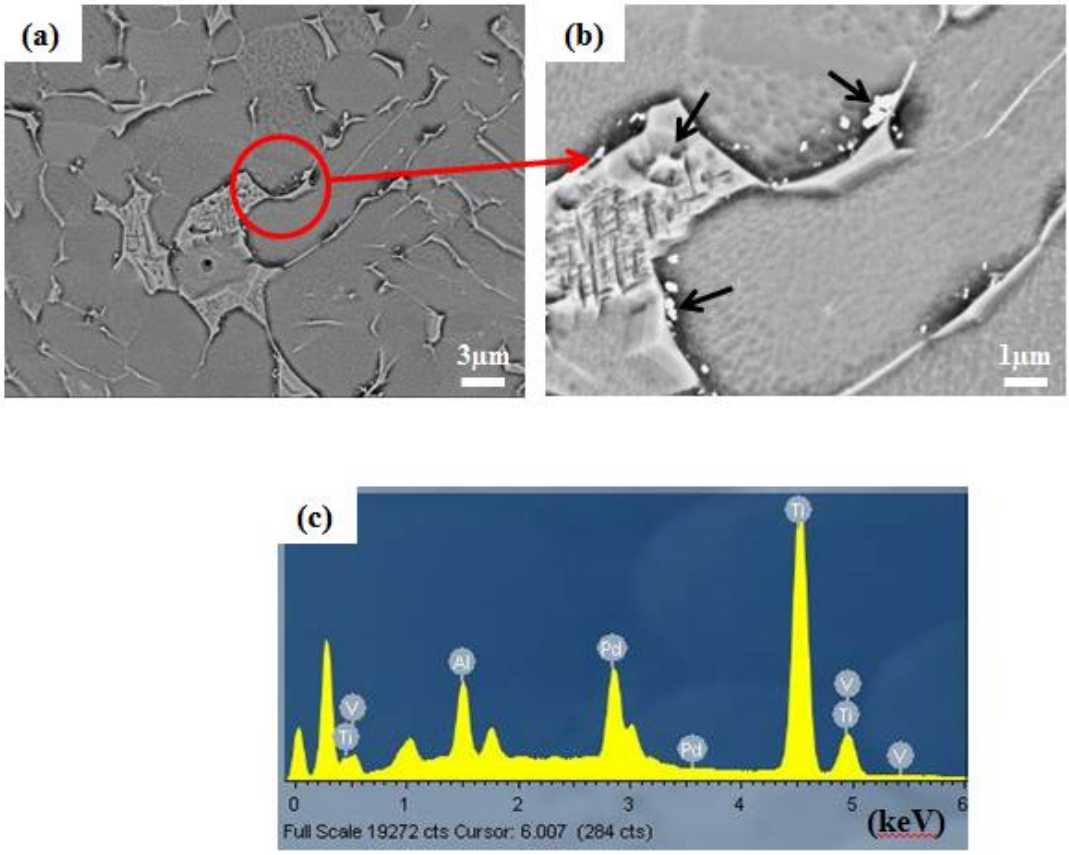

Figure 7 (a-b) Back-scattered electron SEM images showing the microstructure and Pd distribution and morphology in as-HIPed Ti64-0.2Pd sample; (c) EDX spectrum confirming that the bright particles in (b) are Pd particles. The black arrows in (b) point to the Pd particles present at grain boundaries.

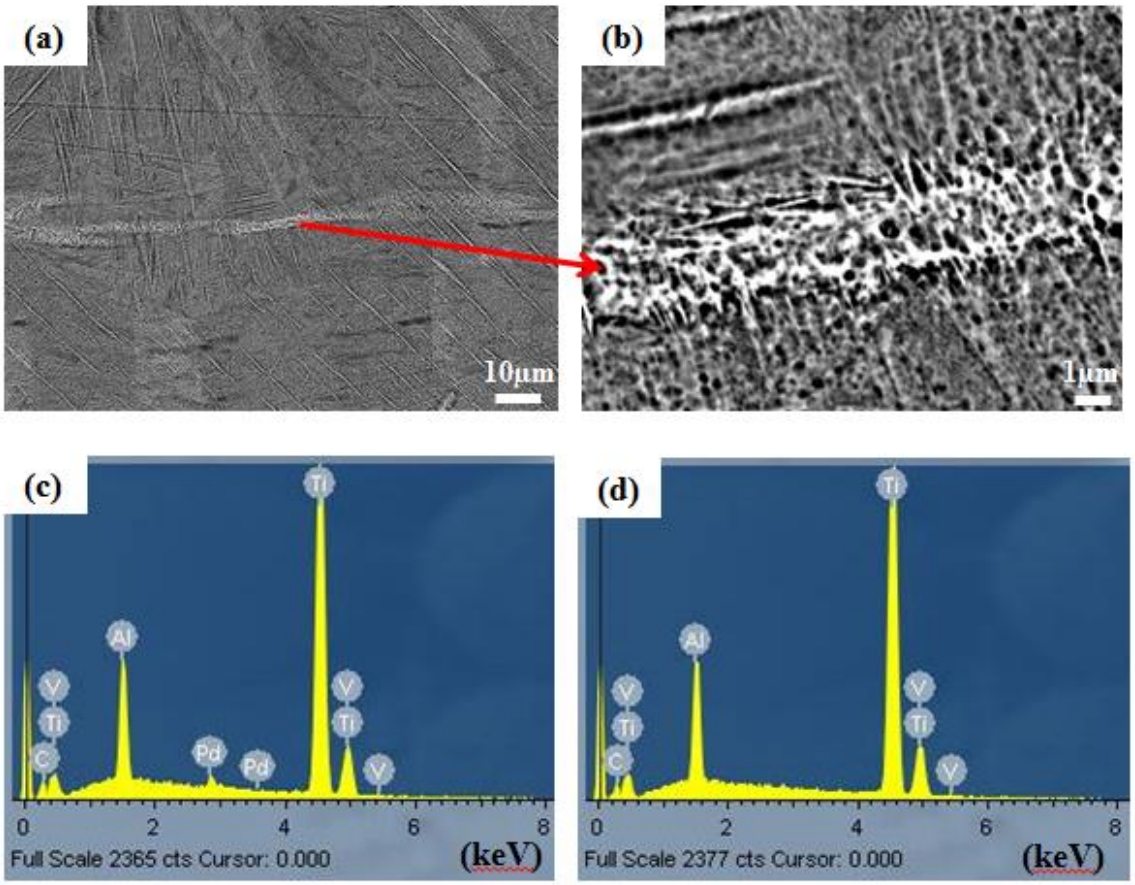

Figure 8 Back scattered electron SEM images showing (a) the microstructure and (b) a region in as-SLMed Ti64-0.2Pd sample where Pd (bright region) can be observed; EDX analysis results for (c) the bright region in (b) and (d) the matrix area.

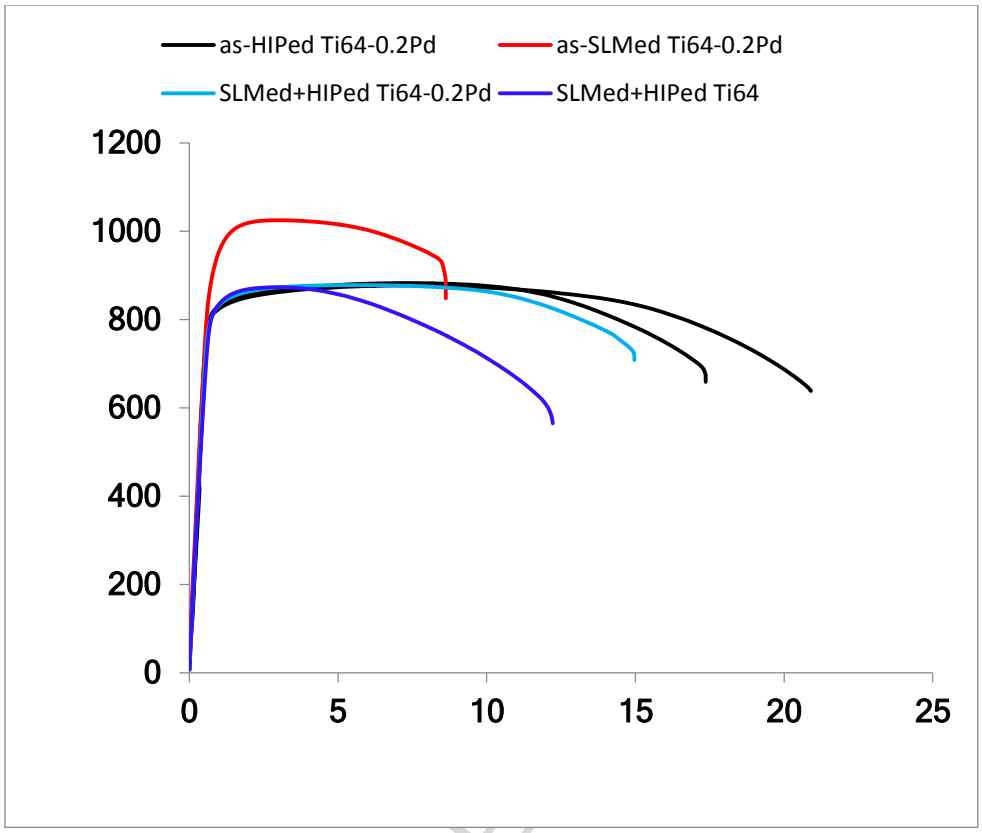

Figure 9 Tensile testing results of Ti64-0.2Pd samples fabricated using different processes. The as-SLMed sample was fabricated at 2300mm/s.

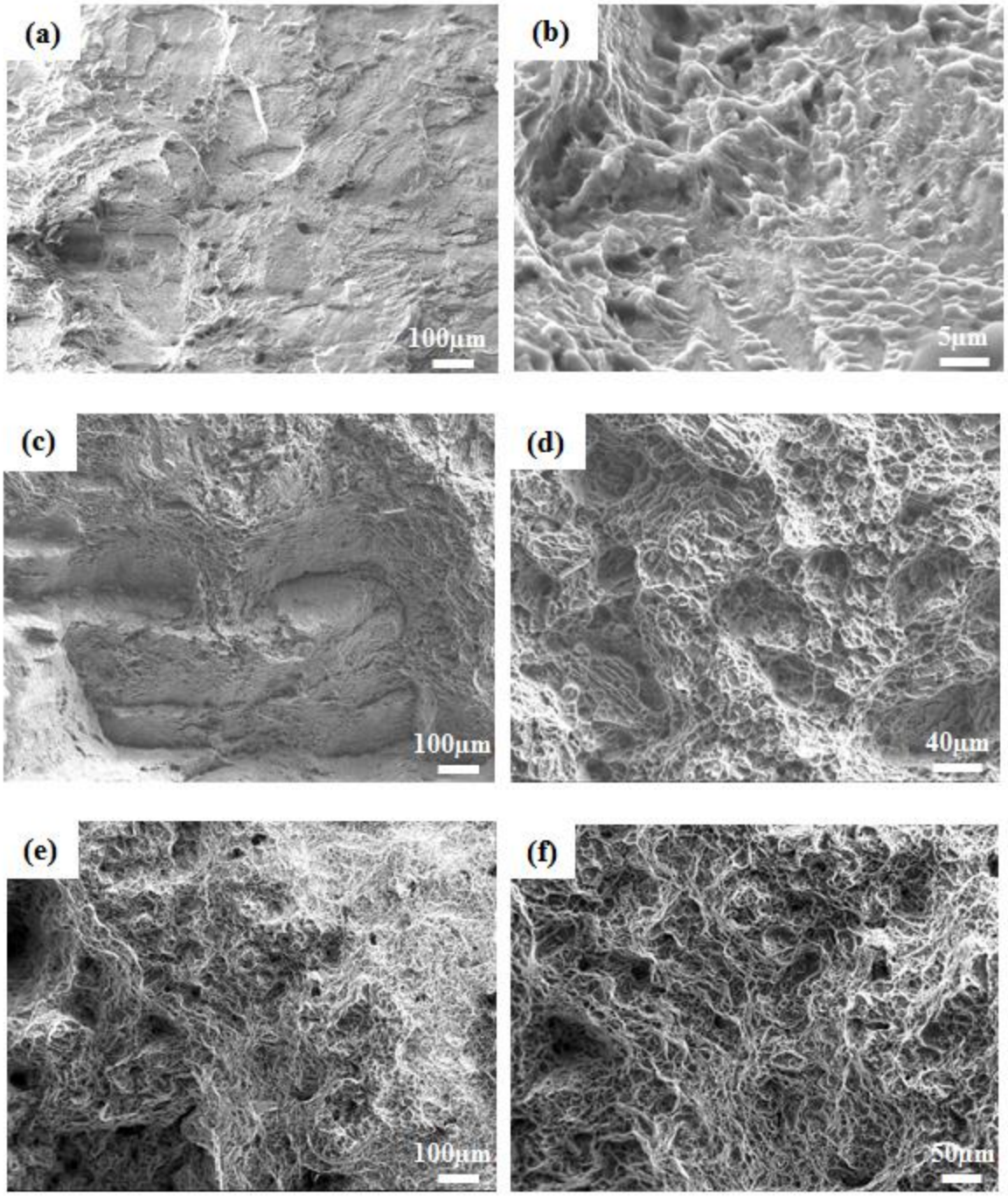

Figure 10 SEM micrographs showing the tensile fracture surfaces of (a-b) as-SLMed (2300mm/s); (c-d) SLMed (3300mm/s) +HIPed; (e-f) HIPed Ti64-0.2Pd samples

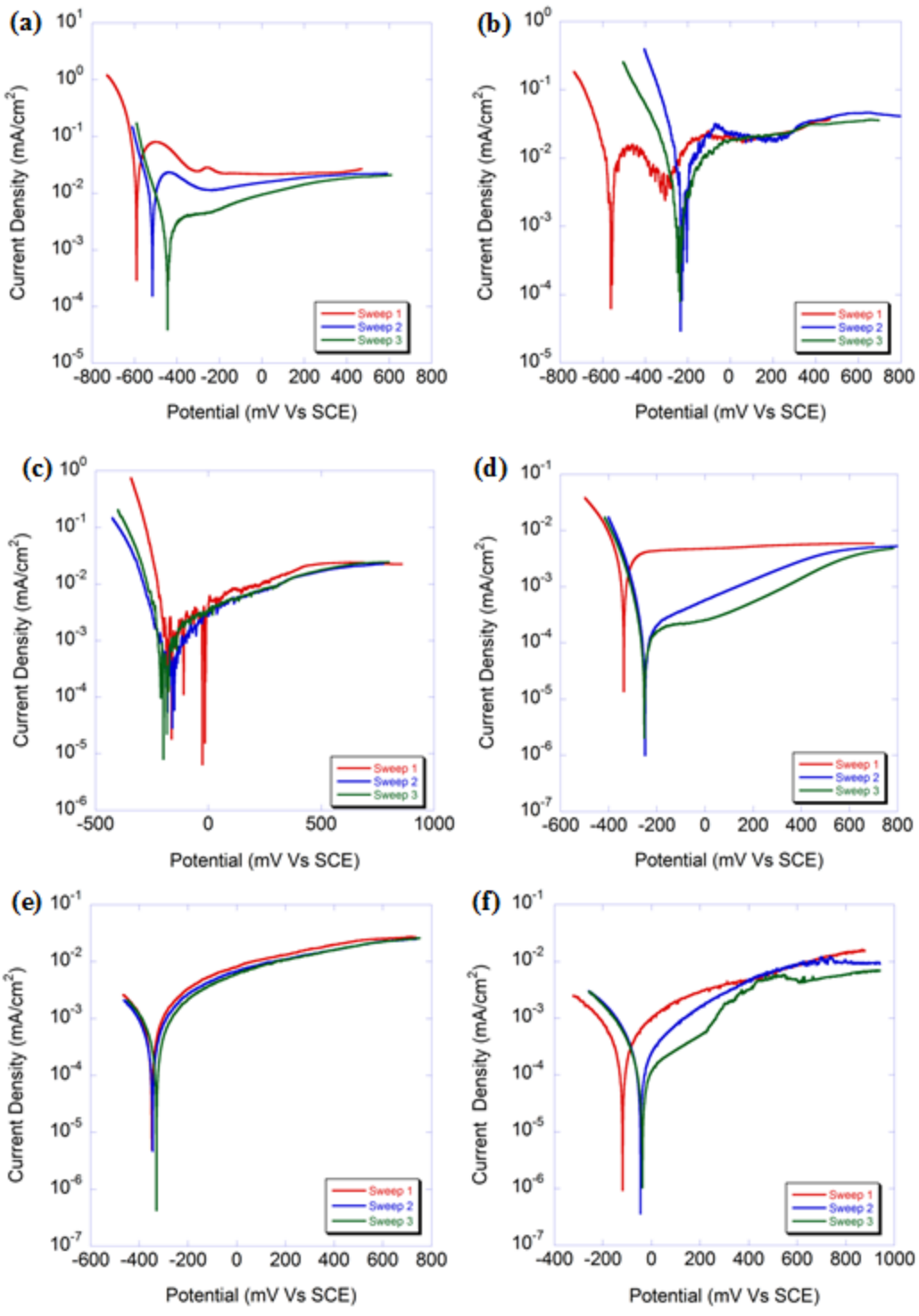

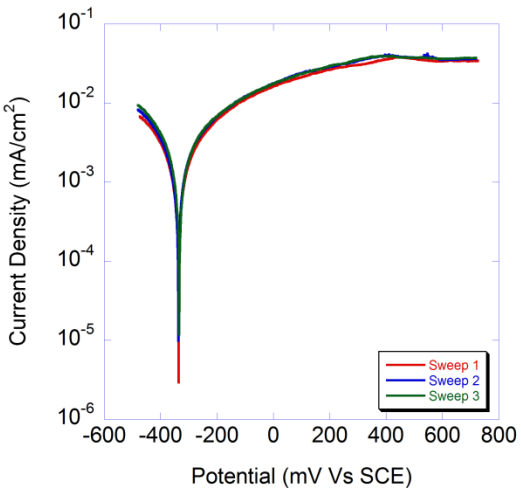

Figure 11 Electrochemical polarisation curves for (a) forged+annealed Ti64; (b) as-HIPed Ti64; (c) as-SLMed Ti64; (d) as-HIPed Ti64-0.2Pd; (e) as-SLMed Ti64-0.2Pd (2300mm/s); (f) as-SLMed Ti64-0.2Pd (3300mm/s); (g) SLMed (3300mm/s)+HIPed Ti64-0.2Pd.

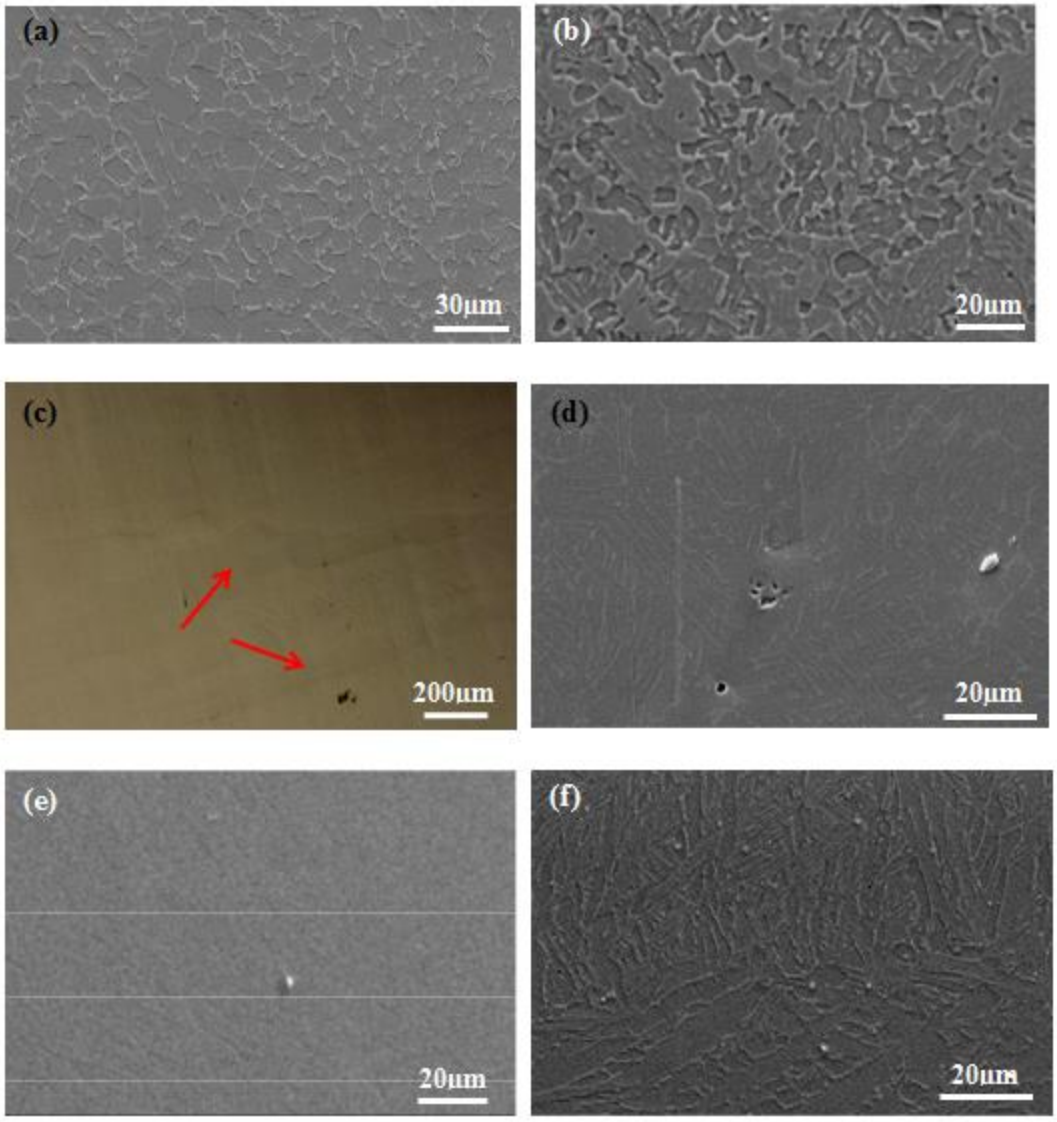

Figure 12 Surface structure of different samples after the electrochemical testing, (a) forged+annealed Ti64; (b) as-HIPed Ti64; (c) as-SLMed Ti64; (d) as-HIPed Ti64-0.2Pd; (e) as-SLMed (2300mm/s) Ti64-0.2Pd; (f) SLMed (3300mm/s)+HIPed Ti64-0.2Pd. The arrows in (c) show that some of the large columnar grains have been corroded away.

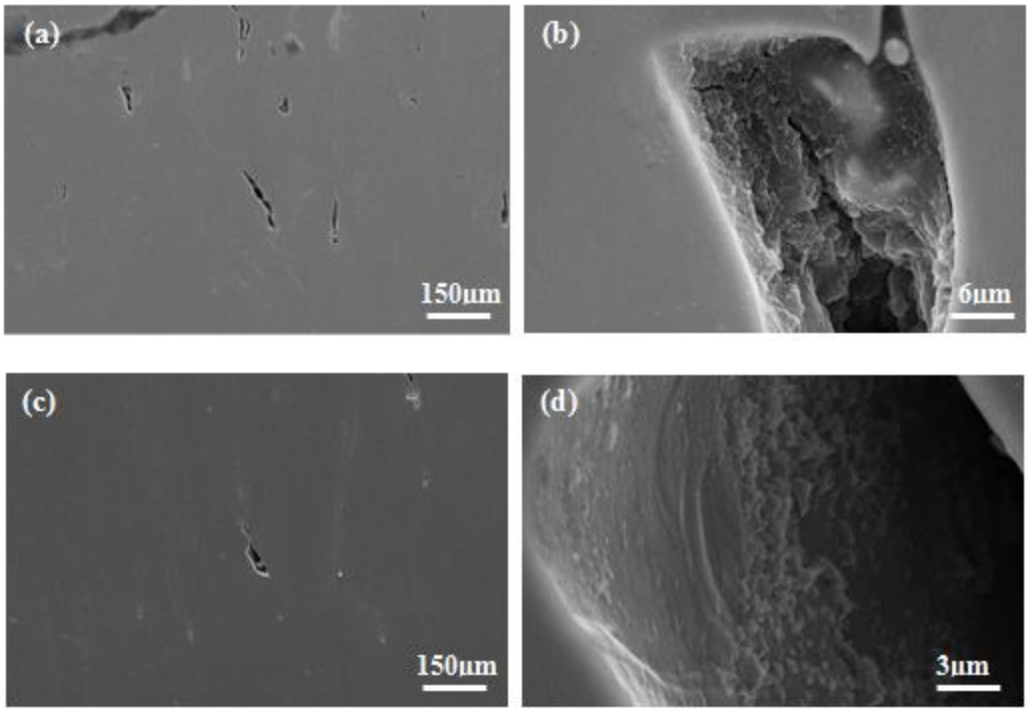

Figure 13 SEM micrographs showing the surface structure of the Ti64-0.2Pd sample fabricated at 3300mm/s (a-b) before and (c-d) after the electrochemical testing

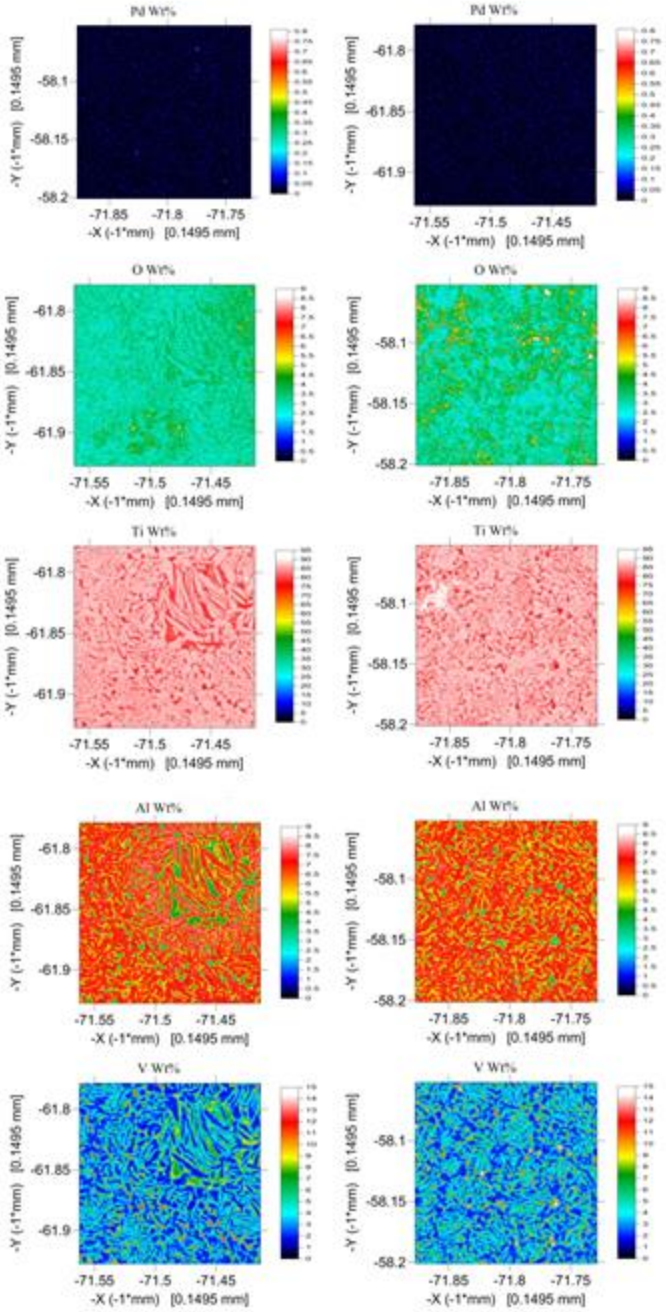

Figure 14 EPMA mapping of as-HIPed Ti64-Pd samples before (left column) and after (right column) corrosion test

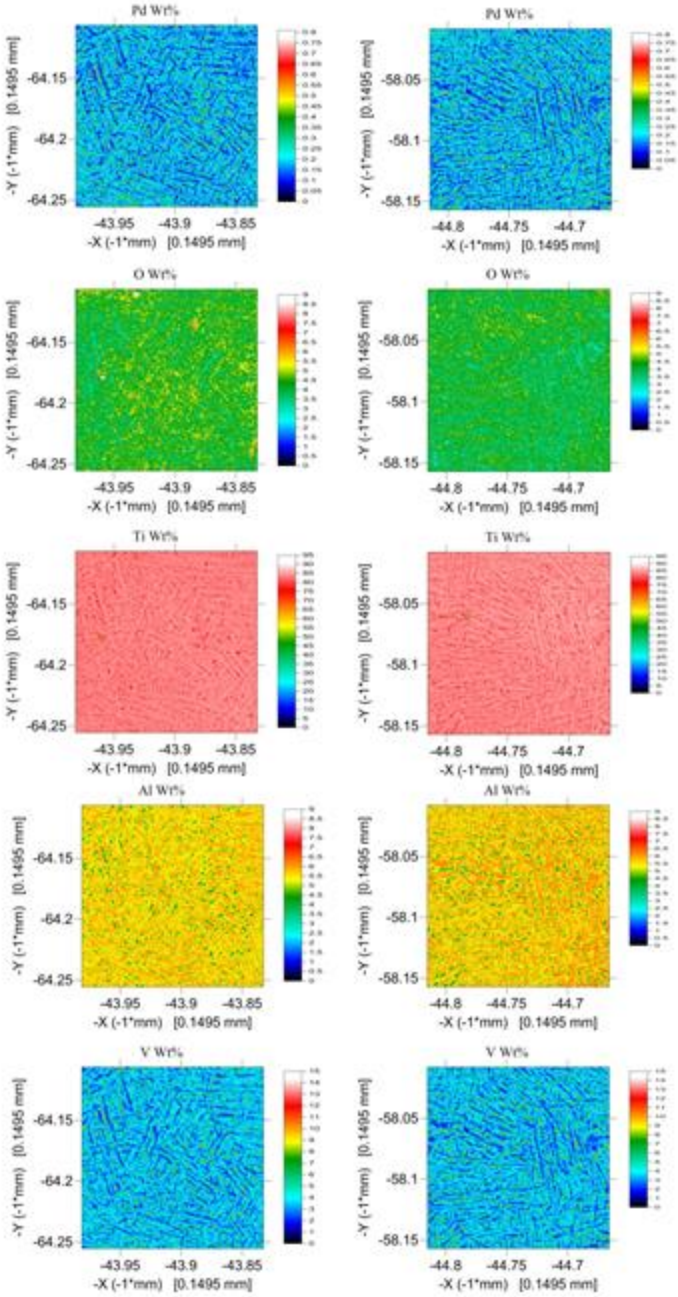

Figure 15 EPMA mapping of as-SLMed Ti64-Pd samples (2300mm/s) before (left column) and after (right column) corrosion test

Graphical abstract

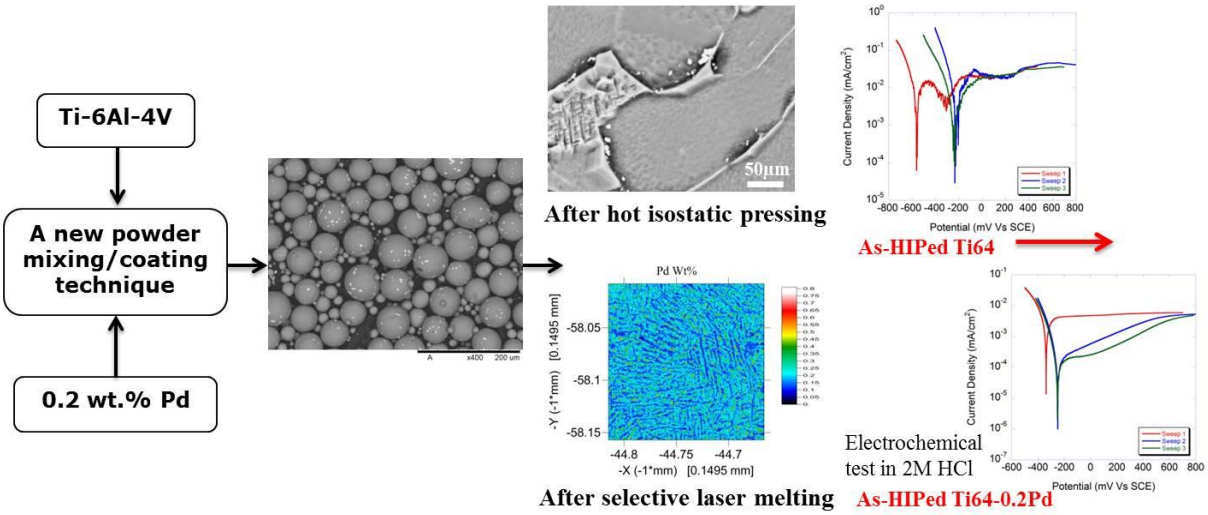

Highlights

- Pd was evenly distributed among Ti-6Al-4V particles using a new mixing technique
- Pd has dissolved completely into Ti-6Al-4V matrix after selective laser melting
- With the addition of Pd, the corrosion resistance of the Ti alloy has been improved
- Coarser grain structure also improves corrosion resistance of the Ti alloy in 2M HCl